Constraints on decaying dark matter

from lensing and magnification of cosmic voids

Earl S. Lester

D.S.U. 2022

12/2022

UNIVERSITY of TASMANIA

Overview

Talk covers recent work with K. Bolejko

1. Lester, E., Bolejko, K. (2021). Imprints of decaying dark matter on cosmic voids. Physical Review D, 104(12), 123540.
2. Lester, E., Bolejko, K. (2022). Constraining decaying dark matter models with gravitational lensing and cosmic voids. In preparation.

Dark matter models

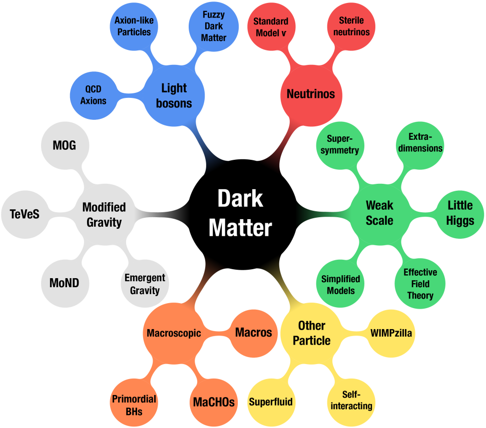

Figure: The myriad models and candidates for dark matter. Image original by Bertone and Tait.

Dark matter models: Zoom back...

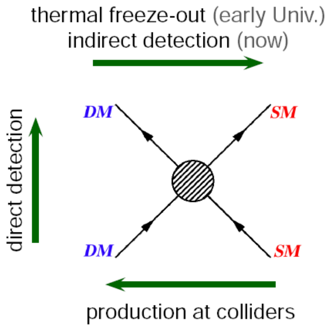

Figure: Simplify the picture by considering interactions (and detection methods).

Dark matter matter: Zoom back...

$$T^{ab}_{(i)\,;b} = I^{a}_{(i)}\,. \tag{1}$$

Our approach

Take a semi-tetrad approach:

$$g_{ab} = \mathbf{e}_a \cdot \mathbf{e}_b = \eta_{ab} \, , \tag{2}$$

with fluid 4-velocity:

$$u_a = \mathbf{e}_0 \, , \tag{3}$$

and spatial axis of symmetry

$$z_a = \mathbf{e}_1 \, . \tag{4}$$

Our approach

Decompose covariant derivative of 4-velocity:

$$u_{a;b} = \omega_{ab} + \sigma_{ab} + \frac{1}{3}\Theta h_{ab} - A_a u_b \, , \tag{5}$$

where

$$h_{ab} = g_{ab} + u_a u_b \, , \tag{6}$$

is a projection tensor.

Multi-fluid models

Multi-fluid total energy momentum tensor:

$$T^{ab} = T^{ab}_{ddm} + T^{ab}_{dm} + T^{ab}_{r} + \ldots \tag{7}$$

Simply eg.

$$T^{ab} = \rho u^a u^b + \eta v^a v^b \,, \tag{8}$$

with

$$v^a = \gamma(u^a + V^a) \,. \tag{9}$$

Multi-fluid models

Giving

$$T^{ab} = \mu u^a u^b + p h^{ab} + 2q^{(a} u^{b)} + \pi^{ab}. \tag{10}$$

with

$$\mu = \rho + \gamma^2 \eta \tag{11}$$

etc.
Furthermore

$$Q \sim \gamma^2 \eta V, \quad p \sim \Pi \sim \gamma^2 \eta V^2 \tag{12}$$

where

$$V^a = V z^a \tag{13}$$

etc.

Titled

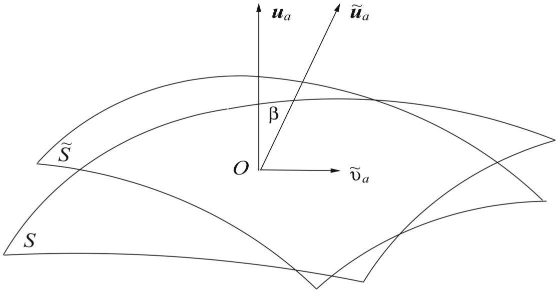

Fig. 1 Observer (O) moving with peculiar velocity $\tilde{v}_a$ (where $\tilde{v}^2 \ll 1$ in our case), relative to the Hubble flow. The 4-velocities u_a and $\tilde{u}_a$, with a hyperbolic (tilt) angle β between them, respectively define the reference frame of the smooth universal expansion and that of the peculiar motion (see Eq. (1)). The 3-D hypersurfaces S and $\tilde{S}$ are normal to u_a and $\tilde{u}_a$ and they respectively define the rest-spaces of the idealised observers and of their real counterparts

Figure: Figure 1 from [4] schematically representing the tilted multi-fluid model.

With interactions

Introduce fluid interactions as:

$$T^{ab}_{(i)\,;b} = I^{a}_{(i)} \,. \tag{14}$$

A model of decay is

$$I^{a}_{(1)} = -\Gamma\rho(u^{a} + w^{a})\,, \tag{15}$$

where

$$w^{a} = \frac{4}{\pi^{2}} v_i \delta z^{a} \tag{16}$$

with δ is the fluid density perturbation, v_i the initial velocity after decay, Γ is the decay-rate.

The formalism leads to the governing equations (among many others)

$$\dot{\mu} = -\Theta\mu - Q' - Q\alpha - 2AQ\,, \tag{17}$$

$$\dot{\rho} = -\Theta\rho - \Gamma\rho\,, \tag{18}$$

$$\dot{Q} = -(\Sigma + \frac{4}{3}\Theta)Q - \mu A\,, \tag{19}$$

where $\dot{X} = u^a X_{;a}$, $X' = z^a X_{;a}$, $\alpha = h_{ab} z^a_{;b}$ and $A \neq 0$.

Zoomed out:

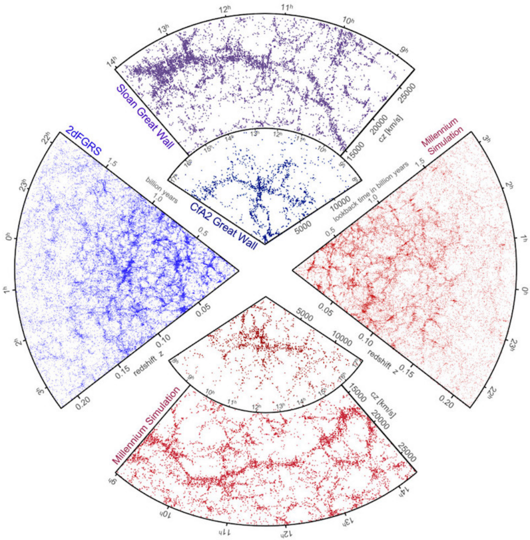

Figure: Credit to C. Burke

Zoom in.... A realistic void:

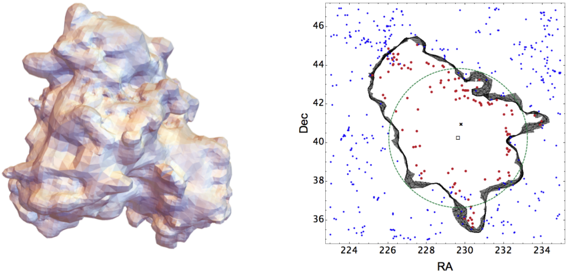

Figure 3. *Left*: A 3-dimensional representation of the bounding surface of an example void from the CMASS catalogue, obtained using the surface information described in Sec. 3.3.4. This void has effective radius $R_v = 86.7\,h^{-1}$Mpc, effective ellipticity $e = 0.05$, $\delta_{g,\mathrm{min}} = -0.93$ and $\overline{\delta}_g = -0.18$. *Right*: A thin slice through the void at redshift $z = 0.528$ is shown by the black 'ribbon'. Points show the projected positions of galaxies lying within a slice of thickness $30\,h^{-1}$Mpc centred at this redshift, with void member galaxies shown with the larger (red) points. The void minimum density centre and the volume-weighted barycentre of its member galaxies are shown by the black square and cross respectively. The green dashed line is the circle projected on the sky by an equivalent sphere of radius R_v.

Figure: Borrowed from [3].

An idealised void:

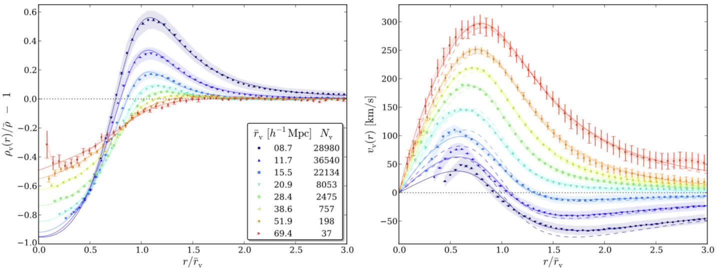

FIG. 1 (color online). Stacked density (left) and velocity (right) profiles of voids at redshift zero in eight contiguous bins in void radius with mean values and void counts indicated in the inset. Shaded regions depict the standard deviation σ within each of the stacks (scaled down by 20 for visibility), while error bars show standard errors on the mean profile $\sigma/\sqrt{N_v}$. Solid lines represent our best-fit solutions from Eq. (2) for density and from Eqs. (4) and (6) for velocity profiles. Dashed lines show the linear theory predictions obtained from evaluating the velocity profile equation at the best-fit parameters obtained from the density stacks.

Figure: Borrowed from [1].

A simplistic void:

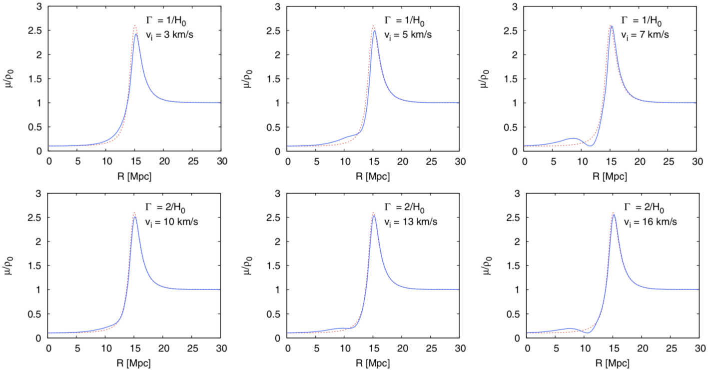

FIG. 1. Density profile at $z = 0$ of the evolved S-type void with (blue solid lines) and without (red dashed lines) decay, for various combinations of the parameters Γ and v_i. This panel clearly illustrates the injection-velocity-dependent growth of novel secondary structure at the edge of the underdense region.

Figure: Taken from [2].

Weak gravitational lensing

Weak-lensing magnification:

$$\mu = 1 + 2\kappa \,, \tag{20}$$

Convergence:

$$\kappa = \frac{\Sigma}{\Sigma_C} \,, \tag{21}$$

Surface mass density:

$$\Sigma = \int \bar{\rho}\, \delta(r(\theta, z))\, d\ell \,. \tag{22}$$

Weak gravitational lensing, 1.

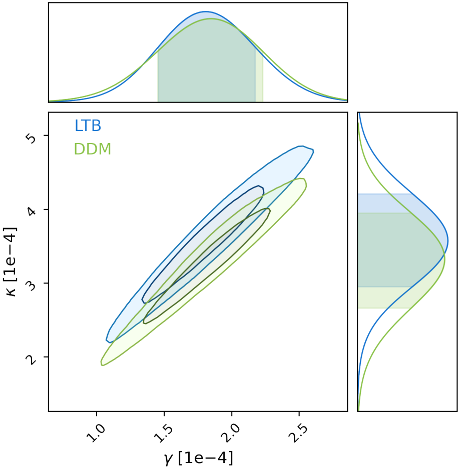

Figure: Small (~ 20 Mpc) voids with (DDM, $v_i \sim 100\,\mathrm{kms}^{-1}$) and without (LTB) decay.

Weak gravitational lensing, 2.

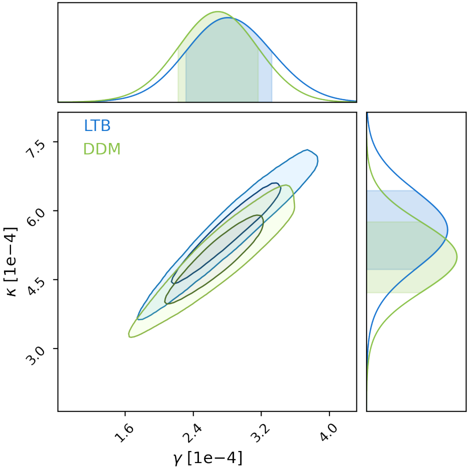

Figure: Large ($\sim$ 30 Mpc) voids with (DDM $v_i \sim 100\,\mathrm{kms}^{-1}$) and without (LTB) decay.

Weak gravitational lensing, 3.

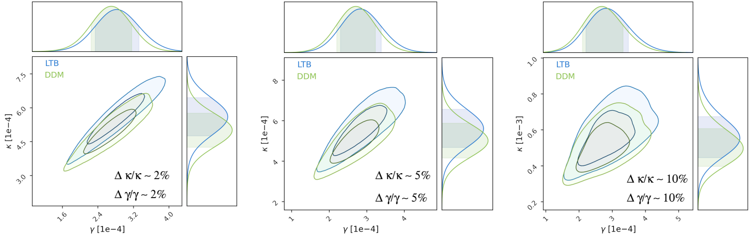

Figure: Demonstrating the effect of increasing uncertainties upon the weak-lensing signals.

Doppler magnification

More realistically

$$\kappa = \kappa_{WL} + \kappa_{DM} + \ldots$$

where $\kappa_{DM} \sim v_{pec}$.

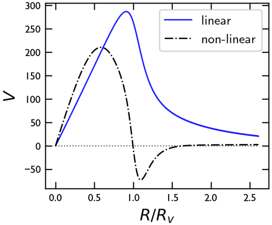

Figure: An example of the peculiar velocities fields around cosmological voids.

References:

N. Hamaus, P. Sutter, and B. D. Wandelt.
Universal density profile for cosmic voids.
Physical review letters, 112(25):251302, 2014.

E. Lester and K. Bolejko.
Imprints of decaying dark matter on cosmic voids.
Physical Review D, 104(12):123540, 2021.

S. Nadathur.
Testing cosmology with a catalogue of voids in the boss galaxy surveys.
Monthly Notices of the Royal Astronomical Society, 461(1):358–370, 2016.

C. G. Tsagas.
The peculiar jeans length.
The European Physical Journal C, 81(8):1–13, 2021.

Questions?